ELSEVIER

Chemical Physics 282 (2002) 451–463

Chemical Physics

www.elsevier.com/locate/chemphys

The distribution of the doped holes in $La_{2-x}Sr_xCu_{1-y}Ru_yO_{4-\delta}$

Z. Hu [a,d,*], M.S. Golden [b], S.G. Ebbinghaus [c], M. Knupfer [a], J. Fink [a], F.M.F. de Groot [e], G. Kaindl [f]

[a] *Institute for Solid State Research, IFW Dresden, P.O. Box 270016, 01171 Dresden, Germany*
[b] *Van der Waals-Zeeman Institute, University of Amsterdam, Valckenierstraat 65, 1018 XE Amsterdam, The Netherlands*
[c] *Lehrstuhl für Festkörperchemie, Institut für Physik, Universität Augsburg, Universitätsstraße 1, 86159 Augsburg, Germany*
[d] *II. Physikalisches Institut, Universität zu Köln, Zülpicher Str. 77, 50937 Köln, Germany*
[e] *Department of Inorganic Chemistry and Catalysis, Utrecht University, 3584 CA Utrecht, The Netherlands*
[f] *Institut für Experimentalphysik, Freie Universität Berlin, Arnimallee 14, 14195 Berlin-Dahlem, Germany*

Received 21 February 2002

Abstract

We present a systematic study of the perovskite-related system $La_{2-x}Sr_xCu_{1-y}Ru_yO_{4-\delta}$ using Cu $L_{2,3}$, Ru $L_{2,3}$, and O K X-ray absorption spectroscopy (XAS), magnetic and electrical measurements. This system can be regarded as hole-doped via substitution of La by Sr and to be electron-doped via substitution of Ru by Cu, and thus the question as to the distribution of the charge carriers and the interaction between Cu and Ru ions are central to our understanding of these novel systems. The comparison of the experimental data with the crystal-field-multiplet calculations shows clearly that the charge balance for $x/2y > 1$ is predominantly achieved by an increase of the Ru valence from Ru(IV) to Ru(V), while Cu remains in the Cu(II) oxidation state. © 2002 Elsevier Science B.V. All rights reserved.

PACS: 78.70.Dm; 71.28.+d; 79.60

1. Introduction

The discovery of high-temperature superconductors (HTSs) [1] has initiated a large number of studies on the system $La_{2-x}Sr_xCuO_4$, which has the simplest crystal structure among the variety of high-temperature superconductors known today. The parent, unsubstituted compound La_2CuO_4 is an antiferromagnetic insulator. Upon Sr-substitution it becomes superconducting with a maximum value of T_c for $x = 0.15$ [2]. At higher doping superconductivity disappears again and $La_{2-x}Sr_xCuO_4$ shows a normal metallic behavior [2]. This has lead to further extensive research of the consequences of substituting the La or Cu atoms by other metals.

Recently, superconductivity was also found in the system Sr_2RuO_4 at rather low temperatures ($T_c \approx 1$ K) [3]. Sr_2RuO_4 is the first non-copper-oxide superconductor with the same K_2NiF_4-type structure as $La_{2-x}Sr_xCuO_4$. Very little is known about

* Corresponding author. Fax: +49-221-470-5178.
E-mail address: zhiwei@ph2.uni-koeln.de (Z. Hu).

PII: S0301-0104(02)00729-2

other members of the $La_{2-x}Sr_xCu_{1-y}Ru_yO_{4-\delta}$ system [4–6], which can be considered to be hole-doped via substitution of La by Sr and electron-doped by the substitution of Ru for Cu. Two previous studies [7,8] indicate that single phase $La_{2-x}Sr_xCu_{1-y}Ru_yO_{4-\delta}$ exists in the regions $0 \leqslant x \leqslant 2$ and $0 \leqslant y \leqslant 1$ with $x \geqslant 2y$ and $x < 1 + 2y$, which are illustrated in the schematic phase diagram of Fig. 1. Two of the most important parameters that control the electronic behavior of these materials are the valences of the Cu and Ru ions. For $\delta = 0$ and $x = 2y$, Cu and Ru have the valence states of Cu(II) and of Ru(IV), as in La_2CuO_4 and Sr_2RuO_4, respectively. For $x > 2y$, thermogravimetric measurements have shown that up to 40% of the Ru or Cu cations adopt a higher oxidation state [7,8], which then is either due to formation of Cu(III) or Ru(V) ions. In the case of high values of the ratio $x/2y$, the system tends to become oxygen-deficient. This leads finally to a breakdown of the K_2NiF_4-type structure when the oxygen deficiency reaches $\delta \leqslant 0.3$ [7]. Within a simple ionic picture copper is in a $Cu^{2+}(3d^9)$ state in La_2CuO_4. Strong tetragonal elongation of the CuO_6 octahedron lifts the degenracy of the e_g orbitals – $d(x^2 - y^2)$ and $d(z^2)$ – with the former being formally half-filled. According to the Zaanen–Sawatzky–Allen classification scheme, La_2CuO_4 is a charge transfer insulator, in which the on-site Coulomb correlation energy U_{dd}, (>8 eV) is greater than the charge transfer energy, Δ [9]. This results in a gap defined by the charge transfer energy between the O 2p and Cu 3d dominated states. Thus, the holes near the Fermi energy (E_F) induced by Sr-doping have mainly O 2p character. In the case of the undoped 4d transition metal oxide Sr_2RuO_4, the Ru $4d^4$ configuration gives rise to metallic behavior, since significant the dispersion of 4d-related states and the strong hybridization between Ru 4d and O 2p states smear out a possible splitting of the t_{2g} orbitals induced by the Jahn–Teller effect. The in plane resistivity has a linear temperature dependence from 20 to 300 K. Energy band structure calculations indicate that three hybridized Ru d–O 2p π bands cross E_F [10,11], where the density of states has mainly Ru 4d character mixed with some O 2p character.

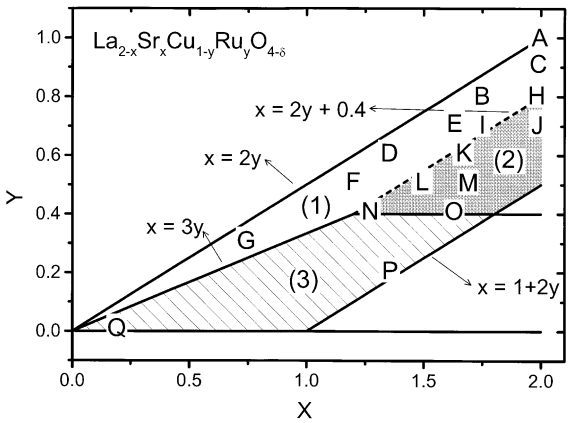

Fig. 1. Schematic phase diagram of $La_{2-x}Sr_xCu_{1-y}Ru_yO_4$, which is divided into three regions for $x > 2y$. The lines $x = 2y$, $x = 3y$ and $x = 2y + 0.4$ make region (1) [light grey shading], where we have the Ru valence $v(\mathrm{Ru}) < 5$ and $\delta = 0$. The lines $x = 2y + 0.4$ and $y = 0.4$ make region (2) [dark grey shading], where we have $v(\mathrm{Ru}) \leqslant 5$ and $\delta \geqslant 0$. The region (3) [hatched] lies below lines $x = 3y$ and $y = 0.4$, where we have $v(\mathrm{Ru}) = 5$ and $\delta > 0$. The capital letters on the diagram indicate the stoichiometry of each sample, as listed in Table 1. For details, see text.

In the mixed Cu/Ru system, the question then arises as to whether for $x > 2y$ charge balance is achieved by hole creation in Cu 3d states, giving rise to Cu(III) ions, or in Ru 4d states resulting in Ru(V). In each case the electronic and magnetic properties are immediately an interesting issue.

Spectroscopic studies using X-ray absorption (XAS) at the Cu $L_{3,2}$ and O K edges are well known to be standard methods for studying Cu valence and the hybridization between Cu 3d and O 2p states in cuprates [12–17]. In addition, our previous combined theoretical and experimental work on model Ru(IV) and Ru(V) oxides indicated that the Ru $L_{2,3}$ XAS spectra – as concerns both their energy position and spectral profile – are sensitive to the valence state of Ru [18]. In this contribution we present a systematic study of the $La_{2-x}Sr_xCu_{1-y}Ru_yO_{4-\delta}$ system using XAS at the Cu $2p_{1/2,3/2}(L_{2,3})$, Ru $2p_{1/2,3/2}(L_{2,3})$, and O 1s (K) thresholds with the aim of answering the above questions. In addition, we have employed magnetization studies to explore whether the system exhibits superconductivity or long-range magnetic order and have carried out electrical resistivity measurements to monitor the effects of the 4d–3d interaction.

2. Experimental

Polycrystalline samples of $La_{2-x}Sr_xCu_{1-y}Ru_yO_{4-\delta}$ were prepared according to the procedures given in [7]. Throughout this contribution, we will refer to the systems in question using capital letters which represent a set of values for x, y and δ denoted (x, y, δ) which are summarized in Table 1. The $Sr_4Ru_2O_9$ sample was prepared as described in [19]. The purity of the compounds was checked using X-ray powder diffraction (XRD). All samples (unless otherwise stated) were found to be single phase. The K_2NiF_4-type structure was verified using Rietveld refinements as shown in Fig. 2. Detailed information regarding these refinements can be found in [7,8].

The magnetic investigations reported here were performed using a SQUID (VTS-905 from Biomagnetic Materials) and were carried out in the temperature range 6–300 K with an external magnetic field of 0.1 T. Electrical resistivity measurements were performed on pressed powder pellets in the temperature range 300–575 K using a standard four-probe technique and a Hewlett-Packard 4284A supply.

Table 1
Ru valence v(Ru) in $La_{2-x}Sr_xCu_{1-y}Ru_yO_{4-\delta}$ as obtained from Eqs. (3)–(5) (see text)

Sample name	X	Y	v(Ru)	δ	Magnetism
A	2	1	4	0	SG
B	1.76	0.8	4.20	0	SG
C	2	0.9	4.22	0	SG
D	1.36	0.6	4.27	0	SG
E	1.64	0.7	4.34	0	SG
F	1.2	0.5	4.40	0	SG
G	0.74	0.3	4.47	0	AF
H	2	0.8	4.50	0	SG
I	1.76	0.7	4.51	0	SG
J	2	0.7	4.57	0.1	SG
K	1.68	0.6	4.67	0.04	SG
L	1.5	0.5	4.80	0.05	SG
M	1.7	0.5	4.80	0.15	SG
N	1.28	0.4	5	0.04	CW
O	1.64	0.4	5	0.22	CW
P	1.36	0.2	>5	0.28	CW

δ was obtained from thermogravimetric measurements. SG, AF and CW denote spin-glass, antiferromagnetic and Curie–Weiss magnetic behaviour, respectively.

The combined thermogravimetric/mass spectrometric measurements were carried out using a Netzsch STA 409 thermoanalytic system connected to a Balzers QMG 421 mass spectrometer by a capillary coupling system. In these experiments about 50 mg of material was heated to 1000 °C at a rate of 10 °C/min under a constant flow of 50 ml/min forming gas (N_2/H_2 95:5%).

The O K and Cu $L_{2,3}$ XAS spectra were recorded at BESSY (Berlin) using the SX700/II monochromator. The O K and Cu $L_{2,3}$ XAS spectra were recorded in fluorescence yield (FY) and total electron yield (TEY) modes, respectively. At the O K and Cu L_3 thresholds, the experimental resolutions were 0.2 and 0.5 eV, respectively. Prior to the measurements, the sample surfaces were scraped in situ with a diamond file at a base pressure of 5×10^{-10} mbar. The O K and Cu $L_{2,3}$ XAS spectra were normalized to the beam current. In addition, the O K data have been corrected for the energy-dependent incident X-ray flux and for self-absorption effects according to a procedure described elsewhere [20,21].

For systems built up of corner sharing of CuO_4 plaquettes (180° Cu–O–Cu interaction pathway), the spectral features from a Cu(III) state should lie ~10 eV above the main peak as a weak, broad satellite [15,22,23]. In contrast to the preliminary work of some of us [24] – in which only the main peak in Cu L_3 XAS spectra were presented and the satellite structures for the $\underline{2p}\ 3d^9$ final state were not shown – now we measured both the Cu L_3 and Cu L_2 spectra, thus not missing out on any important information. CuO was used for energetic calibration at the Cu $L_{2,3}$ and O K thresholds after each injection into the storage ring. A long acquisition time was used for samples with low Cu concentration, for example B(1.76; 0.8, 0) and C(2, 0.9, 0) to improve the signal-background ratio [25].

The Ru $L_{2,3}$ XAS spectra were recorded in transmission geometry at the EXAFS-II beamline at HASYLAB, using a Si(1 1 1) double-crystal monochromator. This resulted in an experimental resolution of $\cong 0.8$ eV (FWHM) at the Ru L_3 threshold (2838 eV). Depending on the Ru content, 5–10 mg of the material in question was

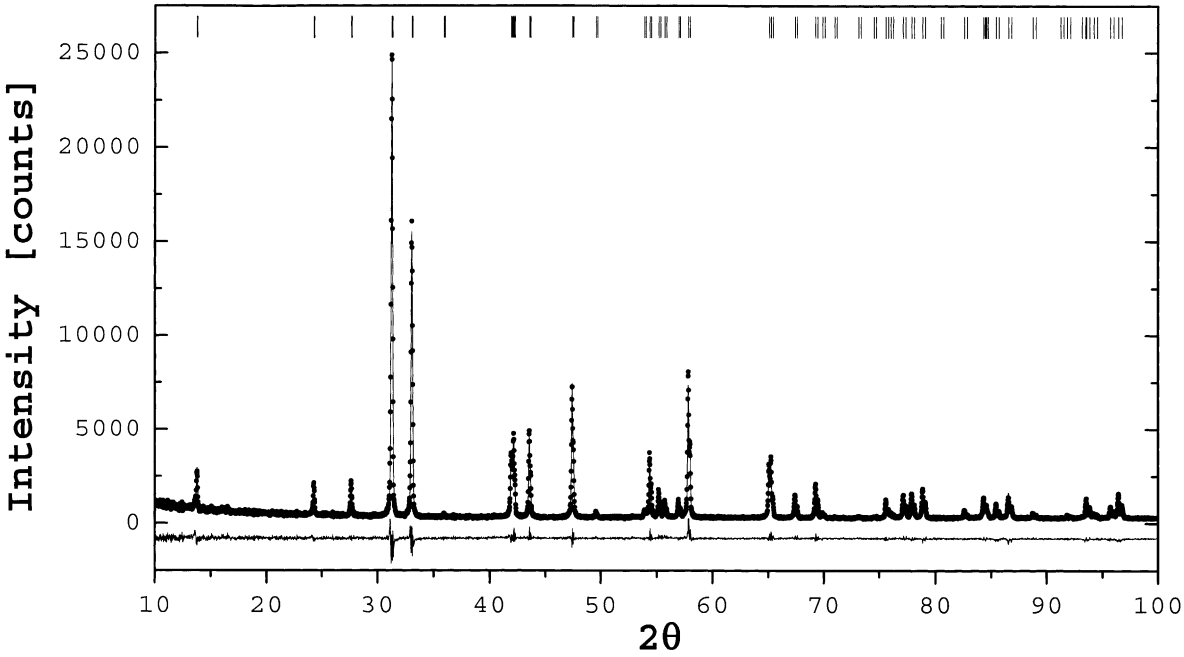

Fig. 2. Rietveld refinement data for the $La_{0.36}Sr_{1.64}Cu_{0.3}Ru_{0.7}O_{4-\delta}$ sample.

mixed with 20 mg polyethylene powder and pressed into a pellet of 13 mm diameter.

3. Results

3.1. Magnetism and conductivity

A large variation of the magnetic properties was found in the system $La_{2-x}Sr_xCu_{1-y}Ru_yO_{4-\delta}$. In this paper, only three typical examples are shown. A more extended study will be published elsewhere. As can be seen from Fig. 3, the sample P(1.36, 0.2, 0.28) (dashed curve) shows an almost ideal Curie–Weiss (CW) behavior in the magnetic susceptibility between 6 K and room temperature, which represents the magnetic behavior found for most of the samples studied. In a number of samples, e.g. E(1.64, 0.7, 0) in Fig. 3, the magnetic susceptibility, χ_{mol}, shows a markedly different behavior below 20 K, depending on whether the sample is field-cooled or zero-field-cooled. The data indicate a typical spin-glass (SG) behavior which had been observed previously by Kim et al. for the series $LaSr_nCuRuO_{n+5}$ (with $n = 1, 2, 3$) [6]. The third class of magnetic behavior is shown for the sample G(0.74, 0.3, 0) in Fig. 3, which shows an antiferromagnetic phase (AF) transition at

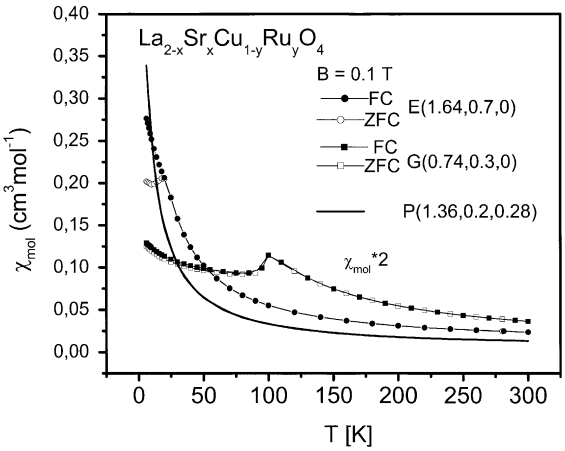

Fig. 3. Magnetic susceptibility, χ_{mol}, of $La_{2-x}Sr_xCu_{1-y}Ru_yO_{4-\delta}$, showing a Curie–Weiss behavior for P(1.36, 0.2, 0.28) (solid line), a spin-glass behavior for E(1.64, 0.7, 0) (filled circles for field-cooled and open circles for zero-field-cooled), and an antiferromagnetic transition at $T_N \approx 117$ K for G(0.74, 0.3, 0) (filled squares for field-cooled and open squares for zero-field-cooled).

$T_N \approx 117$ K. Below T_N the field-cooled and the zero-field-cooled curves are only slightly split. This class of compounds was found to possess an unusually large a axis and a short c axis [7]. The magnetic properties of studied compounds are summarized in Table 1. The electrical resistivity, ρ, exhibits a maximum at $y \approx 0.5$ for a given x, in agreement with previous work [6], where an increase of ρ with y in the region $y < 0.5$ had been reported. This could be a consequence of the disorder induced by the randomly distributed Cu and Ru atoms in the $(Cu,Ru)O_2$ planes. Along a similar vein, it has been found that metallic Sr_2RuO_4 can be driven insulating through changes in doping in $Sr_2Ir_{1-x}Sr_xO_4$ [26]. Previously, $La_{0.5}Sr_{1.5}Cu_{0.5}Ru_{0.5}O_4$ and $La_{0.25}Sr_{1.75}Cu_{0.5}Ru_{0.5}O_4$ have been prepared with the aim of obtaining metallic formal Ru(V) oxides [5]. However, these systems were found to be semiconducting and there was no evidence for the existence of long-range magnetic order.

3.1.1. Thermogravimetry

The reduction of the different samples started between 300 and 450 °C and was finished between 650 °C and 900 °C. As the reaction temperature strongly depends on both the chemical composition and the morphology of the samples (in particular the particle size), we were unable to find a systematic relationship between the start or end temperatures and the values of x, y and δ, respectively. The mass spectra (monitored simultaneously) indicated that H_2O was the only volatile reaction product. This is an important additional information as weight losses due to the evolution of other gases (e.g., CO_2 from unreacted carbonates) would have led to incorrect values of δ. In addition, the absence of such signals can be taken as an additional confirmation of the sample quality.

From the weight loss during reduction and the known values of x and y, the oxygen deficiency δ can easily be calculated. Fig. 4 shows a plot of δ as a function of x for various samples with $y = 0.1$, 0.3, 0.5 and 0.7, respectively. From repeated measurements of selected samples we estimate the error in δ to be approximately ± 0.03. From Fig. 4 it can be seen that for small ratios of x/y the oxygen content is close to the value of 4. On increasing this ratio, the structure starts to become oxygen deficient. The dependence of δ on x and y can well be approximated by the following formulae:

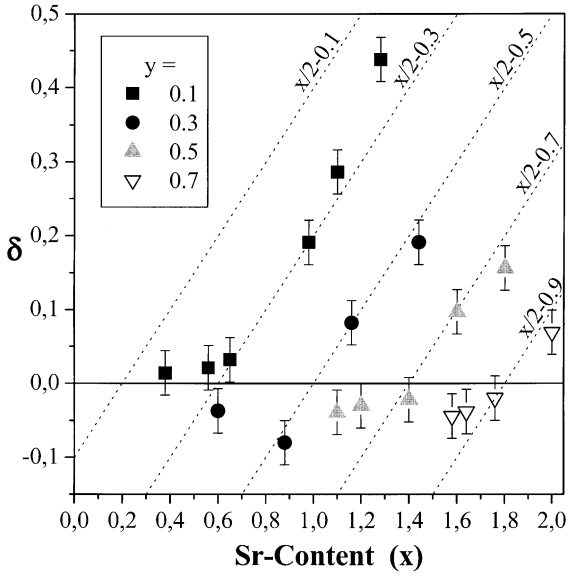

Fig. 4. Dependence of the measured oxygen deficiency δ on x and y. Dotted lines indicate the expected values for. $\delta = x/2 - y - 0.2$. Error bars represent the estimated error of ± 0.03.

$$\delta \approx 0 \quad \text{for } x \leqslant 2y + 0.4 \tag{1}$$

$$\delta \approx x/2 - y - 0.2 \quad \text{for } x > 2y + 0.4. \tag{2}$$

For values of $\delta > 0.3$ the K_2NiF_4 structure becomes unstable and impurity peaks can be found in the XRD patterns. For example, a sample with $x = 1.28$, $y = 0.1$, already contained minor impurity phases visible in the XRD traces. Therefore, it is not surprising that this sample shows a deviation from the above relationship as can be seen in Fig. 4.

3.2. Cu $L_{2,3}$ XAS spectra

Fig. 5 shows the Cu $L_{2,3}$ XAS spectra of some selected compounds of the series $La_{2-x}Sr_xCu_{1-y}Ru_yO_{4-\delta}$, together with those of CuO and $La_2Li_{0.5}Cu_{0.5}O_4$ as Cu(II) and Cu(III) references, respectively. The strong single peak observed for all $La_{2-x}Sr_xCu_{1-y}Ru_yO_{4-\delta}$ systems lies at energies

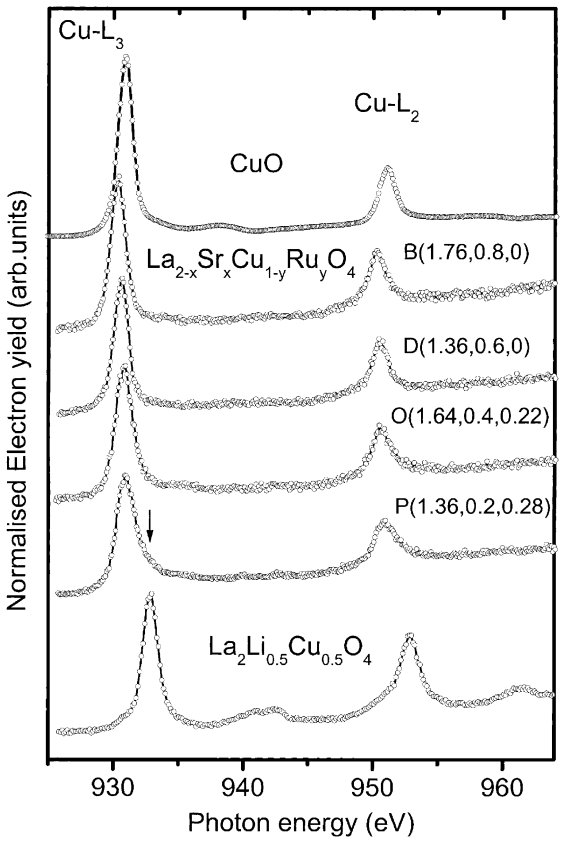

Fig. 5. Cu $L_{2,3}$ XAS spectra of selected $La_{2-x}Sr_xCu_{1-y}Ru_yO_{4-\delta}$ compounds together with spectra of CuO and $La_2Li_{0.5}Cu_{0.5}O_4$ as Cu(II) and Cu(III) references, respectively.

ranging from 930.7 to 931.4 eV, and is shifted by only $|\Delta E| \leqslant 0.3$ eV with respect to that of CuO at 931.2 eV for most of the samples. Sample B(1.76, 0.8, 0) is one exception with a 0.5 eV shift to lower energy. We attribute this larger shift to strong excitonic effects [12], which is a reasonable supposition considering the narrow linewidth for this oxide. The single peak in CuO is assigned to a $\underline{2p}\ 3d^{10}$ final state arising from the $3d^9$ initial state of Cu(II). In contrast, the strong peak in the Cu(III) reference compound $La_2Li_{0.5}Cu_{0.5}O_4$ lies 1.7 eV above the peak of CuO and is attributed to a predominantly $\underline{2p}\ 3d^{10}$ L final state (L denotes a hole in the O 2p ligand orbitals). The weak satellite at ~9 eV above the main peak in $La_2Li_{0.5}Cu_{0.5}O_4$ is assigned to a predominantly $\underline{2p}\ 3d^9$ final state, which thus exhibits multiplet splitting [13,17,22]. The Cu $L_{2,3}$ edges therefore clearly reveal that in most compounds discussed here the copper ions remain divalent [Cu(II)]. Only at very high $x/2y$ ratios in region 3 of Fig. 1 (i.e., close to the breakdown of the K_2NiF_4-type structure) such as for P(1.36, 0.2, 0.28), can one see a weak shoulder (indicated by an arrow in Fig. 5) at the energy of the main peak of $La_2Li_{0.5}Cu_{0.5}O_4$. Such a weak shoulder has also observed previously in $La_{2-x}Sr_xCuO_4$ [12,14,27], where the holes in CuO_2 plane created by Sr doping have mainly O 2p and only little Cu 3d character. This is a result of the fact that to achieve a $3d^8$ configuration for Cu^{3+} state in a simple ionic description, it would be necessary to overcome the particularly large Coulomb correlation energy U_{dd}. In the case of $La_2Li_{0.5}Cu_{0.5}O_4$, each CuO_4 plaquette (which is isolated from the next CuO_4 plaquette by the Li–O sublattice) has one additional hole. This hole has mainly O 2p character resulting in a dominant $\underline{2p}\ 3d^{10}$ L final state in Cu $L_{2,3}$ XAS. A similar spectral feature has also been found in the Cu(III) oxide $NaCuO_2$ in which a 90° Cu–O–Cu interaction pathway causes the inter-plaquette interaction to be weak, leading to a behavior of analogous that an isolated CuO_4 plaquette [23]. In strong contrast to these quasi isolated $Cu(III)O_4$ plaquette systems, for the Cu(III) oxide $LaCuO_3$ which has an 180° Cu–O–Cu interaction pathway leading to stronger inter-plaquette hopping and metallic conductivity, a double-peaked Cu L_3 structure has been found [22].

3.3. Ru $L_{2,3}$ XAS spectra

The fact that the Cu valence remains essentially unchanged upon Sr doping leads to the conclusion that the Ru ions play the central role as regards the charge balance in these compounds. In the following, we first present our observations as regards the spectral response at the Ru $L_{2,3}$ excitation edge for a change of Ru valence and then give a theoretical interpretation of the data. For 4d transition metal (TM) oxides, the larger band-like character of the 4d states and the weaker Coulomb repulsion energy U_{dd} mean that these systems are generally significantly less dominated by correlation effects than their 3d counterparts.

Thus, it costs less energy to remove a 4d electron from a Ru ion than to remove a 3d electron from a Cu ion. Compared with the situation as regards 3d TM L_2 and L_3 XAS spectra [28], both the experimental and theoretical study of 4d TM $L_{2,3}$ XAS spectra lag far behind. It is usually assumed that the 4d TM $L_{2,3}$ XAS spectra reflect directly the unoccupied 4d orbitals, and thus the spectra have often been interpreted in terms of crystal-field or molecular-orbital theories [29–32]. In the case of O_h local symmetry, it is then expected that the intensity ratio of transitions into the crystal-field-split t_{2g} and e_g states $I(t_{2g})/I(e_g)$ is 0.5 for Ru(IV) [$4d^4$] and increases to 0.75 for Ru(V) [$4d^3$] at both the L_2 and the L_3 edges. Recently, however, it was recognized that the intra-atomic Coulomb interaction and the 4d spin–orbit coupling strongly modify the spectral features in Ru $L_{2,3}$ XAS spectra [18,33], as concerns both their energy position and the intensity ratio of the t_{2g} and e_g-related features. Therefore only a combined experimental and theoretical study in which the model explicitly takes multiplet and spin–orbit coupling effects into account can give reliable information on the valence of Ru.

For simplicity, we first show in Fig. 6 the Ru $L_{2,3}$ XAS spectra of $Sr_2Cu_{1-y}Ru_yO_4$ with $y = 1[A(2,1,0)]$, $0.9[C(2,0.9,0)]$, and $0.7[J(2,0.7,01)]$ together with those of $Sr_4Ru_2O_9$ (bottom) as a Ru(V) reference. To ease comparison, the L_2 spectra (open symbols) have been shifted by 129 eV (the Ru 2p spin–orbit splitting) and have been multiplied by 2.1 such that their high energy feature matches the corresponding feature in the L_3 spectra (filled symbols). In each case, the lower and the higher energy component basically reflects transitions into t_{2g} and e_g-related states, respectively. The intensity ratio, $I(t_{2g})/I(e_g)$, is higher at the L_3 edge than at the L_2 edge for the Ru(IV) compound Sr_2RuO_4, but this situation is reversed for the Ru(V) compound $Sr_4Ru_2O_9$. The observed spectral ratios are significantly different from those expected from crystal-field and molecular-orbital theories, as has been discussed in detail in [18]. In addition, on going from Ru(IV) to Ru(V), the energy position of both components of the L_2 and L_3 XAS spectra are shifted by 1.5 eV to higher energies.

The changes in the Ru $L_{2,3}$ XAS spectra occurring upon increasing Ru valence described above can be well reproduced by crystal-field-multiplet calculations (CFMCs) as is shown in Fig. 6. The solid and dashed lines below the spectra of Sr_2RuO_4 and $Sr_4Ru_2O_9$ are the theoretical curves obtained for the L_3 and L_2 edges, respectively. The intensity ratio $I(t_{2g})/I(e_g)$ at both the L_2 and L_3 edges has been found to be very sensitive to the intra-atomic Coulomb interactions, represented by the corresponding Slater integral and to the 4d spin–orbit coupling [18,33]. Considering the strong covalency between the transition metal d and the

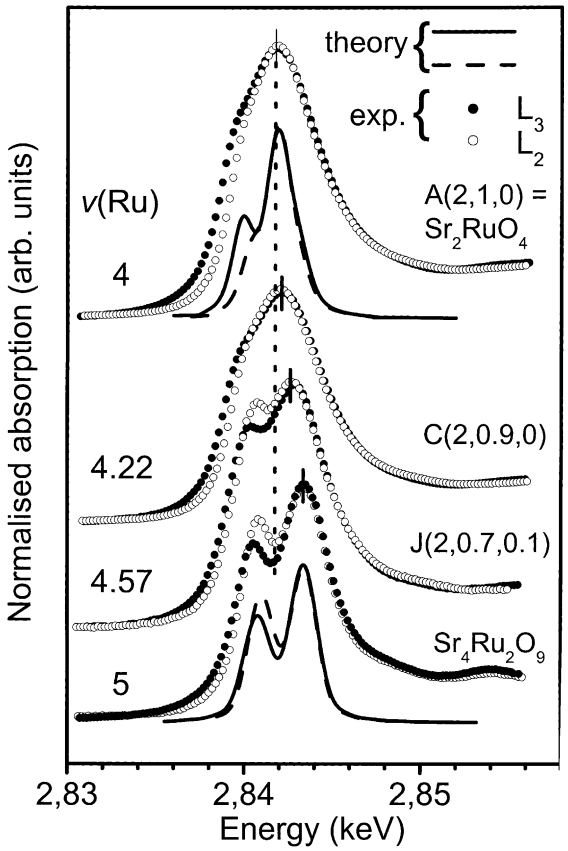

Fig. 6. The XAS spectra of $Sr_2Cu_{1-y}Ru_yO_4$ and of $Sr_4Ru_2O_9$ as a Ru(V) reference at the Ru L_2 edge (open circles) and at the Ru L_3 edge (filled circles). The Ru L_2 data have been shifted and multiplied to overlap with the Ru L_3 data. The theoretical Ru $L_{2,3}$ XAS spectra from crystal-field-multiplet calculations for Ru(IV) and Ru(V) are shown as solid and dashed lines stand for the L_3 and the L_2 edges, respectively. v(Ru) indicates the Ru valence. For details, see text.

O 2p states in these systems, the Slater integrals have to be reduced to 50% and 15% of their atomic values for Ru(IV) and Ru(V), respectively. The 4d spin–orbit coupling is also very important. Neglecting it, the t_{2g}-related peak for the Ru(IV) $4d^4$ configuration (Sr_2RuO_4) should disappear [18], and the intensity ratio $I(t_{2g})/I(e_g)$ should be stronger at L_3 than at L_2 for the Ru(V) system ($Sr_4Ru_2O_9$) which is plainly not the case. On the basis of the experimental and theoretical spectra for the simple, La-free Ru(IV) and Ru(V) systems, we can thus conclude that the upward shift in energy position and the significantly larger $I(t_{2g})/I(e_g)$ ratio at the L_2 compared to the L_3 edge indicate an increase of the Ru valence with increasing Cu concentration in the $Sr_2Cu_{1-y}Ru_yO_4$ system.

We now move on to the more complicated $La_{2-x}Sr_xCu_{1-y}Ru_yO_{4-\delta}$ systems. Firstly, we have calculated the spectra of the $4d^4$ and $4d^3$ systems as a function of the crystal field 10 Dq within a large region and found the intensity ratios to be relatively insensitive to the value of 10 Dq. Thus, as a first step, we estimated the crystal field parameter for the Ru(IV) and Ru(V) systems from the O K XAS spectra. As regards the Ru L XAS spectra, the important parameter in the simulation of the experimental spectra is the degree of reduction of the Slater integrals, which reflects a significant bandwidth of the 4d states and strong Ru 4d and O 2p covalence.

Bearing in mind Eqs. (1) and (2) introduced above to approximate the thermogravimetric data on the oxygen deficiency δ in $La_{2-x}Sr_xCu_{1-y}Ru_yO_{4-\delta}$, and remembering that the Cu ions remains essentially divalent, the ratio $n(V) = N[\mathrm{Ru(V)}]/\{N[\mathrm{Ru(V)}] + N[\mathrm{Ru(IV)}]\}$, where $N[\mathrm{Ru(V)}]$ and $N[\mathrm{Ru(IV)}]$ are number of Ru(V) and Ru(IV) ions, respectively, is obtained by

$$n(V) = x/y - 2 \quad \text{for } x \leqslant 2y + 0.4, \tag{3}$$

$$n(V) = 0.4/y \quad \text{for } x > 2y + 0.4. \tag{4}$$

The Ru valence $v(\mathrm{Ru})$ is then given by

$$v(\mathrm{Ru}) = 4 + n(V). \tag{5}$$

The values of $v(\mathrm{Ru})$ obtained from to Eqs. (3)–(5) are summarized in Table 1. Now we can go back to the phase diagram shown in Fig. 1. The thermogravimetric data indicate that there are three regions for $x > 2y$. The lines $x = 2y$, $x = 3y$ and $x = 2y + 0.4$ make region (1), in which we have the Ru valence $v(\mathrm{Ru}) < 5$ and $\delta = 0$. In this region the holes are located only in the RuO_6 units with both $\mathrm{Cu}(t_{2g}^6e_g^3)-\mathrm{Ru}(t_{2g}^4e_g^0)$ and $\mathrm{Cu}(t_{2g}^6e_g^3)-\mathrm{Ru}(t_{2g}^3e_g^0)$ interactions.

The lines $x = 2y + 0.4$ and $y = 0.4$ delineate region (2), where $v(\mathrm{Ru}) \leqslant 5$ and $\delta \geqslant 0$. In this region only the $\mathrm{Cu}(t_{2g}^6e_g^3)-\mathrm{Ru}(t_{2g}^3e_g^0)$ interaction is achieved in some compounds, such as N(1.28, 0.4, 0.04) and O(1.64, 0.4, 0.22). Anion vacancies are expected to have weaker effects on the low-lying Ru t_{2g} manifolds than on the high-lying Cu e_g^* orbitals. The vacancies will lead to a redistribution of electron density from z^2 band to $x^2 - y^2$ band [5]. The electronic structure of both compounds are very similar to that of $La_{0.5}Sr_{1.5}Cu_{0.5}Ru_{0.5}O_4$ and $La_{0.25}Sr_{1.75}Cu_{0.5}Ru_{0.5}O_{4-\delta}$ studied previously, in which attempts to observe metallic conductivity by doping-induced introduction of the $\mathrm{Ru}(t_{2g}^3e_g^0)$ configuration had failed [5]. Thus, considering this fact together with the above mentioned resistivity data, it would appear that itinerant electronic transport is hindered by the presence of Cu–O–Ru–O–Cu pathways.

Region (3) in Fig. 1 lies below the lines $x = 3y$ and $y = 0.4$ and we have $v(\mathrm{Ru}) = 5$ and $\delta > 0$. In this region the holes can be located in the CuO_4 plaquattes as in the case of $La_{2-x}Sr_xCuO_4$, however, the charge hopping is suppressed by the Cu–O–Ru–O–Cu interaction pathways as discussed above. The Ru valences of 4.22 for C(2, 0.9, 0) [region (1)] and 4.57 for J(2, 0.7, 0.1) [region (2)] are consistent with the conclusion presented here that the Ru valence increases with increasing Cu concentration in the $Sr_2Cu_{1-y}Ru_yO_{4-\delta}$ system.

The Ru $L_{2,3}$ spectra of the more complicated $La_{2-x}Sr_xCu_{1-y}Ru_yO_{4-\delta}$ compounds ($x \neq 0$ and $y \neq 0$) are shown in Fig. 7 with increasing ruthenium valence from top to bottom. One can clearly see a shift of the peak position to higher energy and an increase of the $I(t_{2g})/I(e_g)$ intensity ratios at the Ru L_2 edge with increasing Ru valence. In the case of the sample N(1.28, 0.4, 0.04), the Ru is pentavalent i.e., $n(V) = 1$, with the spectral fea-

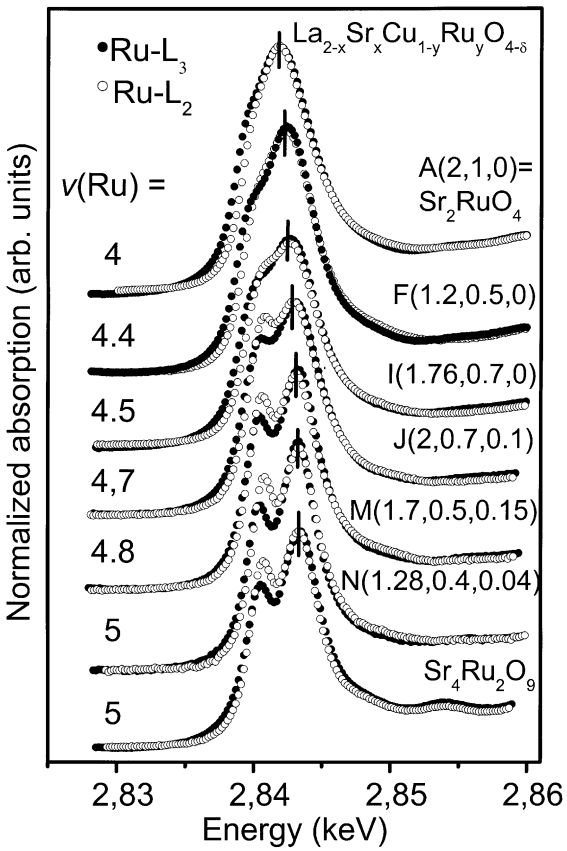

Fig. 7. Ru $L_{2,3}$ XAS spectra of selected $La_{2-x}Sr_xCu_{1-y}Ru_yO_4$ compounds together with that of $Sr_4Ru_2O_9$ as a Ru(V) reference. The v(Ru) values indicate the Ru valence. The Ru L_2 data have been shifted and multiplied to overlap with the Ru L_3 data. For details, see text.

tures [both as regards the energy position and $I(t_{2g})/I(e_g)$] being the same as those of the Ru(V) reference compound $Sr_4Ru_2O_9$. In the foregoing, we have observed that the intensity ratio $I(t_{2g})/I(e_g)$ in the L_2 XAS spectra is the most sensitive spectral parameter to monitor an increase in Ru valence on going from Ru(IV) to Ru(V). This is a result of the larger intensity transfer from the e_g-related to the t_{2g}-related peak in the Ru L_2 XAS spectrum (as compared to the Ru-L_3 spectrum), which in turn is due to the differences in the intra-atomic interactions in the Ru(IV) [$4d^4$] and Ru(V) [$4d^3$] configurations, as shown in the theoretical spectra of Fig. 6. We stress that this spectral behavior is unexpected from crystal-field or molecular-orbital theories of the Ru $L_{2,3}$ XAS, which predict the same ratio for the L_2 and L_3 spectra.

According the rules [Eqs. (1) and (2)] set up from the thermogravimetric measurements, sample P(1.36, 0.2, 0.28) lies in region (3) of the phase diagram shown in Fig. 1, and thus v(Ru) should be greater than five. However, the experimental Ru $L_{2,3}$ spectrum is identical with with that of sample N(1.28, 0.4, 0.04), which has $v(\mathrm{Ru}) = 5$, being at the border of regions (2) and (3) in the phase diagram. Inspection of Fig. 7 shows that sample N (and thus also P) has a Ru $L_{2,3}$ spectrum essentially identical to that of the simple Ru(V) reference compound $Sr_4Ru_2O_9$. In the case of sample P (formally with a valency greater than pentavalent), the charge balance is in fact achieved by the large oxygen deficit of $\delta = 0.28$ and by a small number of holes located in the CuO_6 octahedra, and seen in the Cu $L_{2,3}$ XAS spectra as a shoulder structure visible in Fig. 5. In both Figs. 6 and 7 one can see a narrowing of the both t_{2g}- and e_g-related peaks in the Ru $L_{2,3}$ edges as the Ru valence increases. The reason for this might be that Cu(II) and Ru(IV) are Jahn–Teller ions, causing distortions of the metal–oxygen octahedra of 6–7% and of 27% in Sr_2RuO_4 [10] and La_2CuO_4 [34], respectively. The Jahn–Teller related splitting of e_g into $b_{1g}(d_x^2 - d_y^2)$ and $a_{1g}(d_z^2)$ as well as of t_{2g} into $b_{2g}(d_{xy})$ and $e_g(d_{xz,yz})$ is in fact too small to be experimentally resolved, and thus results only in an extra increase of the linewidth in Sr_2RuO_4. In $La_{2-x}Sr_xCu_{1-y}Ru_yO_{4-\delta}$ a linear decrease of this distortion with increasing Ru valence is expected, since Ru(V) ions (t_{2g}^3) exhibit no Jahn–Teller activity. In the case of J(2, 0.7, 0.1), we have found that $d(B-O_2)/d(B-O_1)$ is reduced to 1%. In Fig. 8 we summarize the energy shifts of the t_{2g}- (filled circles) and e_g-related (closed diamonds) features obtained from the Ru L_3 XAS spectra and the intensity ratio $I(t_{2g})/I(e_g)$ (filled squares) from the Ru L_2 spectra as a function of v(Ru). The open symbols show the values for the Ru(V) reference compound $Sr_4Ru_2O_9$.

3.4. O K XAS spectra

In general, in O K XAS spectra, the correlation effects are much weaker than in the TM $L_{2,3}$ XAS

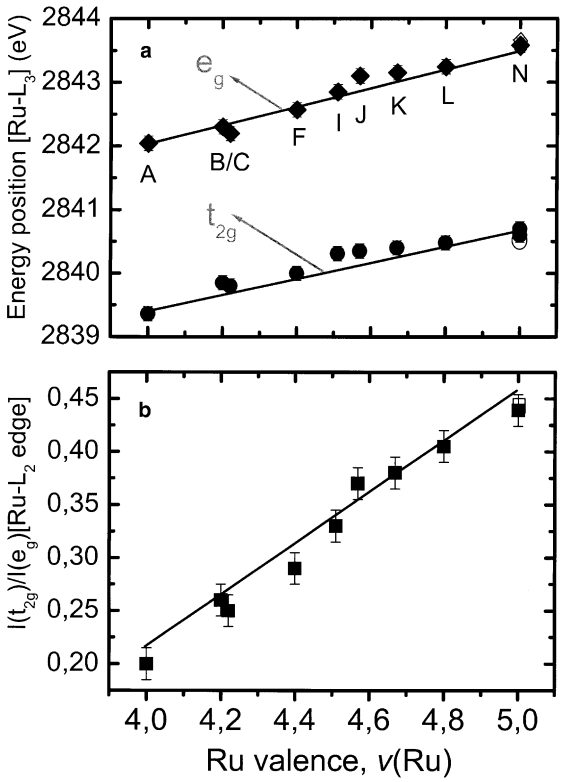

Fig. 8. (a) Energy positions of the t_{2g}-related (filled circles) and the e_g-related (filled diamonds) features in the Ru L_3 XAS spectra and (b) intensity ratios $I(t_{2g})/I(e_g)$ (filled squares) in the Ru L_2 XAS spectra of $La_{2-x}Sr_xCu_{1-y}Ru_yO_4$ as a function of Ru valence. The open symbols show data for the Ru(V) reference compound $Sr_4Ru_2O_9$.

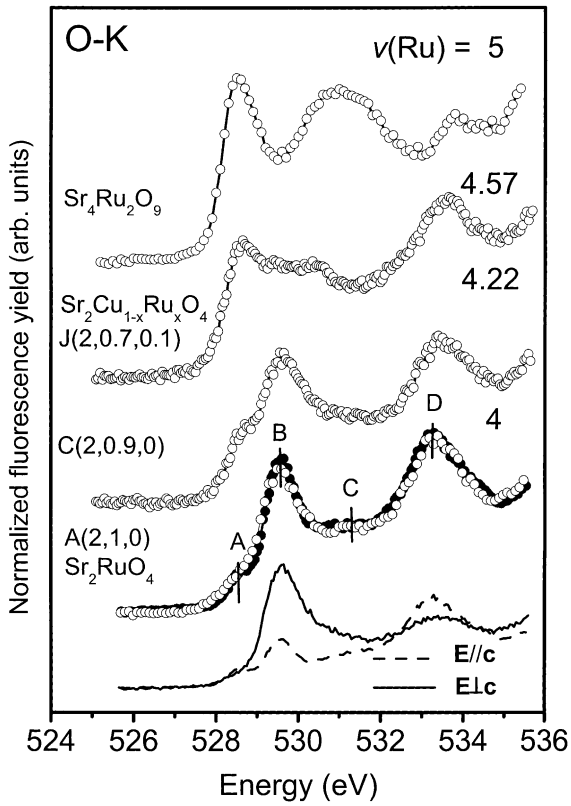

Fig. 9. O K XAS spectra of $Sr_2Cu_{1-y}Ru_yO_4$ with $Sr_4Ru_2O_9$ as a Ru(V) reference.

spectra, i.e., an agreement between the experimental spectra and the results of band structure calculations is plausible [28,35,36]. Therefore, O K XAS spectra are usually studied in order to explore unoccupied states with O 2p character above E_F induced by covalence in the ground state, or by doping-induced hole occupancy of the O 2p states. The O K XAS spectra of $La_{2-x}Sr_xCuO_4$ had been intensively studied previously both experimentally and theoretically in polarization-dependent measurements [12,14,15]. In Fig. 9 the single pre-edge peak in the undoped system La_2CuO_4 (a charge transfer insulator), can be identified with the upper Hubbard band (UHB) i.e., a transition into the empty state ofthe copper $3d(x^2-y^2)$ orbitals which have an admixture of O 2p character. Upon doping, a new electronic state – the Zhang–Rice singlet (ZRS) occurs [37]. This feature is shifted by about 1.5 eV to lower energy with respect to the UHB-related peak, and is often referred to as the doping hole state. From point view of the valence, it has already been mentioned that with increasing valence of the metal ion, the pre-edge peak is shifted to lower energy. In this work we concentrate on the O-K XAS spectral features from the RuO_6 octahedra, where the doped holes are basically trapped.

Considering the splitting of the t_{2g} orbitals in the context of the Jahn–Teller and spin–orbit interactions, one would expect the $\Gamma_8^{1,2}$ and $\Gamma_8^{3,4}$ orbitals to be totally occupied and the $\Gamma_7^{1,2}$ orbital to be empty [18]. However, the Ru 4d states are significantly more extended and more strongly hybridized than Cu 3d states, leading to a larger band dispersion in the Sr_2RuO_4 [10]. The results of

band structure calculations indicate that three bands cut E_F, which falls on the low-energy side (−0.06 eV) of a sharp peak arising from a van Hove singularity (VHS) in the electronic density of states (DOS) [10]. Two holes are found to reside in these bands. The TM-O hybridization results in open shell O 2porbitals leading to the low lying O 2p unoccupied states detected in the O-K XAS spectra. The strong peak B in the O K XAS spectra of Sr_2 RuO_4 in Fig. 9 corresponds to the sharp VHS-related peak in the DOS. The data drawn using open circles are obtained from polycrystalline sample, while the data depicted using filled circles is an isotropic spectrum derived from polarization dependent spectra on the single crystal sample which are shown as solid and dashed lines below the data points for E//c and E//a, respectively. The structure near E_F is found in undoped Sr_2RuO_4 (called 'self-doping') and has predominantly Ru 4d character mixed strongly with O 2p [10]. The weak feature A had been assigned to apical O(2) $2p_x$, O $2p_y$ states hybridized with Ru $4d_{xz}$ and Ru $4d_{yz}$ [25]. According to the band structure calculations [10], the binding energy of O(2) is 1.5 eV smaller than that for the in plane O(1). As stated above, generally, 4d states are more delocalized than 3d states, however, the t_{2g} states are much more localized than the e_g states. The outcome of these competing tendencies is that the low-lying peak B in the Sr_2RuO_4 spectrum is not much different from the pre-edge peak in $La_{2-x}Sr_xCuO_4$. The spectral weight from the e_g-related states is low (see feature C) and in the band structure calculations extends from 1–4 eV above E_F [10,11]. The O K XAS spectra of Sr_2RuO_4 show better agreement with DOS obtained by Oguchi [11] than by Singh [10]. The overall spectral features are very similar to those obtained previously by Schmidt et al. [25]. However, in contrast to the analysis of [25] we wish to point out that structure D at 533.4 eV mainly originates from SrO states. This assignment is supported by the spectrum of $Sr_4Ru_2O_9$, in which the spectral feature from the RuO_6 units is shifted by 1 eV to lower energy upon increasing the Ru valence from Ru(IV) to Ru(V), which results in a better separation of the RuO_6-related state from the SrO band. This shift to lower energy occurs in a manner fully analogous to the behavior observed in the spectra of 3d-TM oxides due to the increase of covalence with increasing valence [16,38]. Thus, the e_g-related peak in $Sr_4Ru_2O_9$ is individually identifiable in the energy range 530.5–532.5 eV. It is evident that the lower energy t_{2g}-related peak at 528.5 eV is narrower than the broad higher energy e_g-related peak as already observed in the Ru $L_{2,3}$ XAS spectrum discussed earlier. This is a direct result of the stronger covalent dpσ-like mixing between the O-2p and Ru-4d(e_g) orbitals. Ru(V) with the $t_{2g}^3e_g^0$ configuration has been known to possess a high spin state ($S = 3/2$) and also shows antiferromagnetic spin order in Ba_2LaRuO_6 [38]. If holes were to be doped into both the CuO_6 and RuO_6 octahedra, the O K XAS spectra of $La_{2-x}Sr_x$-$Cu_{1-y}Ru_yO_{4-\delta}$ would be rather complicated as the UHB structure in La_2CuO_4 lies only 0.8 eV above peak B in Sr_2RuO_4 and the ZRS structure originating from hole doping of the cuprate would strongly overlap with the first pre-edge peak in the Ru(V) oxides. Additionally, this superimposition would occur for both the in-plane and out-of-plane spectral structures in polarization-dependent data. However, if the doped holes are trapped only in the RuO_6 octahedra, the O K XAS spectra would then directly monitor the modification of the hole density interms of the growth of a low lying spectral feature arising solely from the Ru(V)O_6 octahedra. Based upon these considerations, we discuss here only the O K spectra of $Sr_2Cu_{1-x}Ru_xO_4$, since the UHB feature from the Cu(II)O_6 octahedra lies a comfortable 1.8 eV above the Ru 4d t_{2g}-related feature from the Ru(V)O_6 octahedra. The O K spectra of Sr_2Cu_{1-y} $Ru_yO_{4-\delta}$ are shown in Fig. 9. The spectrum of sample C [v(Ru) = 4.22] exhibits a low-energy shoulder visible below the main Ru(IV) t_{2g}-related feature. This shoulder lies at the same energy as the first pre-edge peak in $Sr_2Ru_2O_9$ and thus is assigned to holes in t_{2g} states in Ru(V)O_6 octahedra. On further increasing the v(Ru) to 4.57 (sample J) the Ru(V) t_{2g}-features becomes dominant and the Ru(IV) t_{2g}-related structure overlaps partly with the UHB from the Cu(II)O_6 octahedra and is thus no longer resolvable as a separate peak. From Fig. 9 we can conclude that with increasing Cu concentration in $Sr_2Cu_{1-y}Ru_yO_4$ the Ru

valence increases, as was proven earlier in the context of the Ru $L_{2,3}$ XAS spectra. This leads, then, to the creation of high spin $S = 3/2$ Ru(V) ions, which if considered as 'impurities' will not be beneficial for superconductivity.

4. Summary

From a systematic study of the Cu $L_{2,3}$, Ru $L_{2,3}$, and O K XAS spectra of the system $La_{2-x}Sr_xCu_{1-y}Ru_yO_{4-\delta}$ combining both experiment and theory, we have found that for $x > 2y$, the charge balance upon Sr and Ru doping is achieved by an increase of the Ru valence from Ru(IV) to Ru(V) when going from region (1) to region (3) [via region (2)] of the phase diagram shown in Fig. 1, with a pure Ru(V) valence being reached at the border between regions (2) and (3). At all stages the Cu remains essentially divalent. In region (3) of the phase diagram, Ru remains as Ru(V), and charge balance requirements lead to an oxygen deficit δ and a transfer of holes into the CuO_6 octahedra, before leading finally to a breakdown of the K_2NiF_4-type structure at high δ. Although hole counts of up to 0.2 holes per CuO_6 octahedra can be reached in region (3), these systems are not superconductors. By comparison with data from band structure calculations, we have found that the O K XAS spectra exhibit a larger unoccupied DOS just above E_F in undoped Sr_2RuO_4 than is the case in over-doped $La_{2-x}Sr_xCuO_4$. The doped holes in the $Ru(V)O_6$ octahetra are reflected by the appearance of lower energy structure in the O K XAS spectra by comparison with a simple Ru(V) reference compound.

The lower Coulomb repulsion energy U for Ru than for Cu makes Ru valence fluctuations significantly more favourable in the 4d electron system, resulting in Ru(IV) $\rightarrow$ Ru(V) transitions upon hole doping. The introduction of these high-spin Ru(V) ($S = 3/2$) centers most likely brings with it a strong impurity effect in the mixed $(Cu,Ru)O_2$ planes, which is not beneficial for superconductivity. Indeed, analysis of the electrical resistivity indicate that the presence of Cu–O–Ru–O–Cu interaction pathways mainly suppresses conductivity.

Acknowledgements

We thank F. Grasset and J. Darriet for providing the $Sr_4Ru_2O_9$ sample and the staff of BESSY and HASYLAB for experimental assistance. This work was supported in part by the Deutsche Forshungsgemeinschaft within SFB 463, SFB 484, and SFB 608.

References

[1] J.G. Bednorz, K.A. Müller, Z. Phys. B 64 (1986) 189.
[2] K. Sreedhar, C.N.R. Rao, Mater. Res. Bull. 25 (1990) 1235.
[3] Y. Maeno, H. Hashida, K. Yoshida, S. Nishizaki, T. Fujita, G. Bednorz, F. Lichtenberg, Nature (London) 372 (1994) 32.
[4] K. Ramesha, S. Uma, N.Y. Vasanthacharya, J. Gopalakrishnan, J. Solid State Chem. 128 (1997) 169.
[5] M.P. Attfield, P.D. Battle, S.K. Bollen, S.H. Kim, A.V. Powell, M. Workman, J. Solid State Chem. 96 (1992) 344.
[6] S.H. Kim, P.D. Battle, J. Magn. Magn. Mater. 123 (1993) 273.
[7] S. Ebbinghaus, A. Reller, Solid State Ionics 101–1031 (1997) 369.
[8] S. Ebbinghaus, M. Fröba, A. Reller, J. Phys. Chem. B 101 (1997) 99099.
[9] J. Zaanen, G.A. Sawatzky, J.W. Allen, Phys. Rev. Lett. 55 (1985) 418.
[10] D.J. Singh, Phys. Rev. B 52 (1995) 1358.
[11] T. Oguchi, Phys. Rev. B 51 (1995) 1385.
[12] see e.g. J. Fink, N. Nücker, E. Pellegrin, H. Romberg, M. Alexander, M. Knupfer, J. Electron Spectrosc. Relat. Phenom. 66 (1994) 395.
[13] Z. Hu, C. Mazumdar, G. Kaindl, F.M.F. de Groot, S.A. Warda, D. Reinen, Chem. Phys. Lett. 297 (1998) 321.
[14] C.T. Chen, L.H. Tjeng, J. Kwo, H.L. Kao, P. Rudolf, F. Sette, R.M. Fleming, Phys. Rev. Lett. 68 (1992) 2543.
[15] C.T. Chen, F. Sette, Y. Ma, M.S. Hybertsen, E.B. Stechel, W.M.C. Foulkes, M. Schulter, S.-W. Cheong, A.S. Cooper, L.W. Rupp Jr., B. Batlogg, Y.L. Soo, Z.H. Ming, A. Krol, Y.H. Kao, Phys. Rev. Lett. 66 (1991) 104.
[16] Z. Hu, G. Kaindl, S.A. Warda, D. Reinen, F.M.F. de Groot, B.G. Müller, J. Chem. Phys. 101 (1994) 6570.
[17] G. Kaindl, O. Strebel, O. Kolodziejczky, A. Schäfers, W. Kiems, R. Lösch, S. Kemmler-Sack, R. Hoppe, H.P. Müller, D. Kissel, Physica B 158 (1989) 446.
[18] Z. Hu, H. von Lips, M.S. Golden, J. Fink, G. Kaindl, F.M.F. de Groot, S. Ebbinghaus, A. Reller, Phys. Rev. B 61 (2000) 5262.
[19] C. Dussarrat, J. Formpeyrine, J. Darriet, Eur. J. Solid State Chem. 32 (1995) 3.
[20] L. Tröger, D. Arvanitis, K. Baberschke, H. Michaelis, U. Grimm, E. Zschech, Phys. Rev. B 46 (1992) 3283.

[21] J. Jaklevic, J.A. Kirby, M.P. Klein, A.S. Robertson, Solid State Commun. 23 (1997) 679.
[22] K. Okada, A. Kotani, J. Phys. Soc. Jpn. 68 (1999) 666.
[23] M.S. Golden, C. Dürr, A. Koitzsch, S. Legner, Z. Hu, S. Borisenko, M. Knupfer, J. Fink, J. Electron Spectrosc. Relat. Phenom. 117 (2001) 203.
[24] S. Ebbinghaus, Z. Hu, A. Reller, J. Solid State Chem. 156 (2001) 194.
[25] M. Schmidt, T.R. Cummins, M. Bürk, D.H. Lu, N. Nücker, S. Schuppler, F. Lichtenburg, Phys. Rev. B 53 (1996) R14761.
[26] R.J. Cava, B. Batlogg, K. Kiyono, H. Takagi, J.J. Krajewski, W.F. Peck Jr., L.W. Rupp Jr., C.H. Chen, Phys. Rev. B 49 (1994) 1890.
[27] A. Fujimori, H. Namatame, K. Akeyama, N. Kosugi, Phys. Rev. B 49 (1994) 7193.
[28] F.M.F. de Groot, Doctoral Thesis, Katholieke Universitet Nijmegen, 1991.
[29] C. Sugiura, M. Kitamura, S. Muramatsu, J. Chem. Phys. 84 (1986) 4824.
[30] G.N. George, W.E. Cleland Jr., J.H. Enemark, B.E. Smith, C.A. Kipke, S.A. Roberts, S.P. Cramer, J. Am. Chem. Soc. 112 (1990) 2541.
[31] C. Sugiura, M. Kitamura, S. Muramatsu, J. Phys. Chem. Solids 49 (1988) 1095.
[32] T.K. Sham, J. Am. Chem. Soc. 105 (1983) 2269.
[33] F.M.F. de Groot, Z. Hu, M.F. Lopez, G. Kaindl, F. Guillot, M. Tronic, J. Chem. Phys. 101 (1994) 6570.
[34] V.B. Grande, H. Müller-Buschbaum, M. Schweizer, Z. Anorg. Chem. 428 (1977).
[35] M. Abbate, R. Potze, G.A. Sawatzky, A. Fujimori, Phys. Rev. B 49 (1994) 7210.
[36] A. Fujimori, I. Hase, M. Nakamura, H. Namatame, Y. Fujishima, Y. Tokura, Abbate, F.M.F. de Groot, M.T. Czyzyk, J.C. Fuggle, O. Strebel, F. Lopez, M. Domke, G. Kaindl, Phys. Rev. B 46 (1992) 9841.
[37] F.C. Zhang, T.M. Rice, Phys. Rev. B 37 (1994) 330.
[38] P.D. Battle, J.B. Goodenough, R. Paice, J. Solid State Chem. 46 (1983) 234.